The AKT/GSK3β-Mediated Slug Expression Contributes to Oxaliplatin Resistance in Colorectal Cancer via Upregulation of ERCC1

Wei Wei,*[1] Xiao-Dong Ma,†[1] Guan-Min Jiang,‡ Bin Shi,§ Wen Zhong,¶ Chun-Lei Sun,§ Liang Zhao,* Yan-Jiao Hou,* and Hao Wang*

*Department of Laboratory Medicine, The Affiliated Anhui Provincial Hospital of Anhui Medical University, Hefei, P.R. China
†Department of Medicinal Chemistry, School of Pharmacy, Anhui University of Chinese Medicine, Hefei, P.R. China
‡Department of Clinical Laboratory, The Fifth Affiliated Hospital, Sun Yat-sen University, Zhuhai, P.R. China
§Department of General Surgery, The Affiliated Anhui Provincial Hospital of Anhui Medical University, Hefei, P.R. China
¶Department of Pathology, The Affiliated Anhui Provincial Hospital of Anhui Medical University, Hefei, P.R. China

Although oxaliplatin serves as one of the first-line drugs prescribed for treating colorectal cancer (CRC), the therapeutic effect is disappointing due to drug resistance. So far, the molecular mechanisms mediating oxaliplatin resistance remain unclear. In this study, we found the chemoresistance in oxaliplatin-resistant HCT116 cells (HCT116/OXA) was mediated by the upregulation of ERCC1 expression. In addition, the acquisition of resistance induced epithelial–mesenchymal transition (EMT) as well as the Slug overexpression. On the contrary, Slug silencing reversed the EMT phenotype, decreased ERCC1 expression, and ameliorated drug resistance. Further mechanistical studies revealed the enhanced Slug expression resulted from the activation of AKT/glycogen synthase kinase 3β (GSK3β) signaling. Moreover, in CRC patients, coexpression of Slug and ERCC1 was observed, and increased Slug expression was significantly correlated with clinicopathological factors and prognosis. Taken together, the simultaneous inhibition of the AKT/GSK3β/Slug axis may be of significance for surmounting metastasis and chemoresistance, thereby improving the therapeutic outcome of oxaliplatin.

Key words: Excision repair cross-complementation group 1 (ERCC1); Slug; Drug resistance; Epithelial–mesenchymal transition (EMT); AKT/GSK3β

INTRODUCTION

Colorectal cancer (CRC) is one of the most common human malignant diseases worldwide with increasing incidence and leading rate of mortality. Annually, over 1.2 million new cases of CRC are diagnosed and 608,700 deaths have been documented[1]. As a frequently prescribed drug in the conventional chemotherapy for CRC patients, oxaliplatin exerts its cytotoxicity by generating intrastrand and interstrand DNA–platinum adducts, which inhibits gene transcription and leads to G_2/M cell cycle arrest[2]. Despite its advantage in terms of overall survival rates, the acquired resistance against oxaliplatin has posed a considerable challenge to clinical CRC treatment[3]. Therefore, elucidating the mechanisms underlying the chemoresistance will be meaningful for exploring potential strategies to improve the therapeutic outcome of oxaliplatin.

Increasing evidence has indicated phenotypic and molecular association between epithelial–mesenchymal transition (EMT) and chemoresistance[4–6]. Cancer cells are resistant to chemotherapy when acquiring EMT phenotype[7,8]. Slug, as a zinc finger transcription factor, controls EMT via binding to the E-box site in the promoter of E-cadherin and repressing its transcription[9–11]. In addition to the role in inducing EMT, Slug displays a broad spectrum of biological functions in cancer cells. Transient coexpression of Slug and Sox9 suffices to convert differentiated luminal cells into mammary stem cells with long-term mammary gland-reconstituting ability[12]. Moreover, Slug leads to paclitaxel resistance by antagonizing p53-mediated apoptosis in ovarian cancer cells[13]. These observations illustrated the importance of Slug in sustaining the more aggressive phenotype.

The molecular mechanisms involved in the development of resistance to platinum anticancer drugs are

---

extremely complicated, mainly including the blockage of apoptosis, enhanced DNA repair, reduced cellular accumulation, and intracellular inactivation[14,15]. Excision repair cross-complementation group 1 (ERCC1), a DNA repair protein, has been identified as one of the most pivotal factors, which induces resistance to platinum anticancer drugs via removing platinum-induced DNA adducts[16]. The correlation between ERCC1 and the poor response to platinum anticancer drugs has been implicated in a myriad of tumors[16]. For instance, high expression of ERCC1 contributes to cisplatin treatment failure and is closely linked to the poor prognosis in patients suffering from lung cancer and ovarian cancer[17,18]. However, the mechanisms underlying ERCC1 expression are not yet clearly elucidated.

The present study validated that oxaliplatin-resistant CRC cells displayed EMT features, and a novel pathway, AKT–glycogen synthase kinase 3β (GSK3β)–Slug–ERCC1, was proved to maintain the aggressive phenotype for chemoresistant cancer cells. The findings disclosed in this article may be of significance in overcoming the oxaliplatin resistance

MATERIALS AND METHODS

Chemicals and Reagents

Oxaliplatin was obtained from Sigma-Aldrich (St. Louis, MO, USA). LY294002, SB203580, BAY11-7082, and LiCl were obtained from Beyotime Biotechnology (Shanghai, China). The suppliers and catalog numbers for all primary antibodies used in the study are provided in Table 1. Horseradish peroxidase (HRP)-conjugated secondary antibody, Alexa Fluor 488/594-conjugated secondary antibody, 4′,6-diamidino-2-phenylindole (DAPI), and TRIzol reagent were purchased from Invitrogen (Carlsbad, CA, USA). Lipofectamine 2000 was obtained from Life Technologies (Carlsbad, CA, USA). PrimeScript® RT reagent Kit and SYBR® Premix Ex Taq™ were products of TaKaRa (Dalian, China). Short hairpin RNAs (siRNAs) against human ERCC1 and Slug were obtained from GenePharma (Shanghai, China). The siRNA sequences are as follows: si-negative control, 5′-UUCUCCGAAC GUGUCACGUTT-3′ (sense) and 5′-ACGUGACACGUU CGGAGAATT-3′ (antisense); si-ERCC1-1, 5′-GCCAAG CCCUUAUUCCGAUTT-3′ (sense) and 5′-AUCGGAAU AAGGGCUUGGCTT-3′ (antisense); si-ERCC1-2, 5′-GC GACGUAAUUCCCGACUATT-3′ (sense) and 5′-UAGU CGGGAAUUACGUCGCTT-3′ (antisense); si-Slug-1, 5′-CCCAUUCUGAUGUAAAGAATT-3′ (sense) and 5′-UU CUUUACAUCAGAAUGGGTT-3′ (antisense); si-Slug-2, 5′-GAAUGUCUCUCCUGCACAATT-3′ (sense) and 5′-UUGUGCAGGAGAGACAUUCTT-3′ (antisense).

Cell Culture

The HCT116 and SW480 colorectal carcinoma cell lines were obtained from the Type Culture Collection

Table 1. Antibodies Used in the Study

Antibody	Catalog	Supplier
β-Actin	66009-1-lg	Proteintech Group
ERCC1	14586-1-AP	Proteintech Group
ABCB1	13978T	Cell Signaling Technology
ABCC1	BS7474	Bioworld Technology
ABCC2	24893-1-AP	Proteintech Group
ABCC3	Ab3375	Abcam
ABCC10	Ab91451	Abcam
ABCC12	Ab91453	Abcam
ABCG2	BS3482	Bioworld Technology
BAX	50599-2-lg	Proteintech Group
BCL-2	12789-1-AP	Proteintech Group
GLUT1	Ab652	Abcam
HIF1α	20960-1-AP	Proteintech Group
P27	25614-1-AP	Proteintech Group
P53	10442-1-AP	Proteintech Group
P65	66535-1-lg	Proteintech Group
P38 MAPK	66234-1-lg	Proteintech Group
KLF4	11880-1-AP	Proteintech Group
LAT1	5347T	Cell Signaling Technology
LC3I-II	2775	Cell Signaling Technology
PARP	9542T	Cell Signaling Technology
E-cadherin	60335-1-lg	Proteintech Group
Vimentin	60330-1-lg	Proteintech Group
N-cadherin	22018-1-AP	Proteintech Group
Fibronectin	15613-1-AP	Proteintech Group
α-SMA	55135-1-AP	Proteintech Group
Slug (for WB)	9585T	Cell Signaling Technology
Slug (for IHC)	sc-166476	Santa Cruz
Snail	BS1853	Bioworld Technology
Twist	25465-1-AP	Proteintech Group
ZEB1	21544-1-AP	Proteintech Group
β-Catenin	Sc-7963	Santa Cruz Biotechnology
STAT3	10253-2-AP	Proteintech Group
p-AKT	4060T	Cell Signaling Technology
GSK3β	22104-1-AP	Proteintech Group
p-ERK	4370	Cell Signaling Technology
p-p65	3033	Cell Signaling Technology
p-p38 MAPK	4511S	Cell Signaling Technology
p-GSK3β	9323T	Cell Signaling Technology
Histone H3	A2348	ABclonal
AKT	A7270	ABclonal
ERK	4695T	Cell Signaling Technology

of the Chinese Academy of Sciences (Shanghai, China). Oxaliplatin-resistant HCT116 cells HCT116/OXA were derived in our laboratory. Briefly, parental HCT116 cells were exposed to a series of stepwise increased concentrations of OXA (1, 2, 4, 8, 12, 24, and 48 μM). HCT116 cells were treated with 1 μM OXA for 48 h, and then changed with drug-free culture medium. After the cells returned to normal growth, the same concentration of OXA was added for induction. This process was repeated three times, gradually increasing the OXA concentration. HCT116/OXA cells were cultured in Dulbecco's

modified Eagle's medium (DMEM)/F12 culture medium with 2 μM OXA to maintain their resistance. The culture medium was changed to drug free 48 h prior to the cell used in the experiments. HCT116 cells were maintained in DMEM/F12 culture medium supplemented with 10% fetal calf serum (FBS). SW480 cells were maintained in DMEM culture medium with 10% FBS. The cells were cultured under a humidified 5% CO_2 atmosphere at 37°C in an incubator. MycoGuard™ Mycoplasma PCR Detection Kit (FulenGen, Guangzhou, China) was used to detected mycoplasma infection every 3 months.

Transwell Migration Assay

Cells of different treatment groups (1×10^5/insert) suspended in 150 μl of serum-free culture media were added into the upper chamber, while 600 μl of complete media was added to the lower chamber. After 24 h of incubation, the cells migrated to the lower side of the membrane were fixed in 4% paraformaldehyde for 20 min, stained with hematoxylin, and counted under an upright microscope (five fields per chamber). Each assay was carried out in triplicate and repeated in three independent experiments.

Cell Viability Assay

Cell viability was measured by using the cell counting kit-8 (CCK-8) agent. Briefly, cells of different treatment groups were seeded in 96-well plates at a density of 2×10^4 cells/well and treated with different concentrations of oxaliplatin or cisplatin for 48 h. The 10-μl CCK-8 agent was added to each well, and the plates were incubated for 2 h at 37°C. The absorbance was detected at 570 nm using a microplate reader. All experiments were performed in triplicate.

Quantitative Real-Time Polymerase Chain Reaction (RT-PCR)

Total RNA from cells of different treatment groups was purified using TRIzol reagent according to the manufacturer's guidelines. Then 500 ng of mRNA was generated into complementary DNA (cDNA). Quantification of target genes and the reference [glyceraldehyde-3-phosphate dehydrogenase (GAPDH)] gene was studied in triplicate on ABI-7500 (Applied Biosystems, Carlsbad, CA, USA). The specific primers used in the study are provided in Table 2. Following normalization to GAPDH gene, expression levels for target gene were calculated using the comparative threshold cycle (Ct) method. The ΔCt values were calculated according to the formula ΔCt = Ct (gene of interest) − Ct (GAPDH) in correlation analysis, and the 2−ΔΔCt was calculated according to the formula ΔΔCt = ΔCt (control group) − ΔCt (experimental group) for determination of relative. Data were presented as the mean ± standard deviation (SD) from three independent experiments.

Western Blotting (WB) Analysis

WB assay was performed as previously described[7]. Briefly, the cells of different treatment groups were lysed with WB and immunoprecipitation (IP) lysis buffer (Beyotime Biotechnology). Equal protein samples were loaded in SDS-polyacrylamide gels and then transferred onto polyvinylidene difluoride (PVDF) membranes. After blocking with 5% nonfat milk at room temperature for 2 h, the membranes were incubated with primary antibodies at 4°C overnight and then incubated with secondary antibodies for 1.5 h at room temperature. Specific immune complexes were detected by chemiluminescence reagent (Life Technologies). Band intensity was quantified by densitometry analysis using Image-Pro Plus 4.5 software (Media Cybernetics Inc., Rockville, MD, USA).

Immunofluorescence

The cells of different treatment groups were seeded on chamber slides for 24 h, then washed with phosphate-buffered saline (PBS), fixed with 4% paraformaldehyde for 15 min, and permeabilized with 0.5% Triton X-100 for 10 min. After blocking with goat serum for 2 h at room temperature, cells were incubated with antibodies against E-cadherin, N-cadherin, vimentin, fibronectin, or Slug (1:100 dilution) at 4°C overnight. Slides were washed with PBS and incubated with Alexa Fluor 488- or Alexa Fluor 594-conjugated secondary antibodies (1:1,000 dilution) for 1 h at room temperature. Nuclei were stained with DAPI (10 μg/ml) for 10 min. Samples were examined with confocal laser scanning microscopy (Zeiss, Jena, Germany) to analyze expression and location of these molecules.

Nuclear/Cytoplasm Separation

Nuclear and cytoplasm fractions from cancer cells were obtained by using a nuclear/cytosol fractionation kit (BioVision, Milpitas, CA, USA), and WB analysis was done as described above.

Immunohistochemistry

Seventy-four CRC tumor tissues and 40 adjacent normal tissues were collected from Anhui Provincial Hospital. Sections cut from these tissues were subjected to deparaffinization/rehydration and antigen retrieval by boiling in 0.01 M sodium citrate buffer for 30 min. The sections were blocked with 10% goat serum and then incubated with primary antibodies against Slug and ERCC11 at a 1:200 dilution at 4°C overnight in a humidified chamber. After being washed with PBS, slides were incubated with HRP-conjugated antibody; DAB was used as substrate and Mayer's hematoxylin was applied as counterstain. Throughout the above analyses, controls were prepared by omitting the primary antibodies.

The expression levels of Slug and ERCC1 were independently evaluated by two pathologists. The tumor cells

Table 2. Primers Used in the RT-PCR Assay

Gene	Forward Primer 5′–3′	Reverse Primer 5′–3′
ERCC1	CTGGAGGTGACCAAACTCATCTA	AGTGGGCTTGGTTTTGGTCTGG
ABCB1	TGCTCAGACAGGATGTGAGTTG	AATTACAGCAAGCCTGGAACC
ABCC1	GCCAAGAAGGAGGAGACC	AGGAAGATGCTGAGGAAGG
ABCC2	TGGTGGCAACCTGAGCATAGG	ACTCGTTTTGGATGGTCGTCTG
ABCC3	CTTAAGACTTCCCCTCAACATGC	GGTCAAGTTCCTCTTGGCTC
ABCC4	GGTTCCCCTTGGAATCATTT	AATCCTGGTGTGCATCAAACAG
ABCC5	ACCCGTTGTTGCCATCTTAG	GCTTTGACCCAGGCATACAT
ABCC6	GTGGTGTTTGCTGTCCACAC	ACGACACCAGGGTCAACTTC
ABCC10	ATTGCCCATAGGCTCAACAC	AGCAGCCAGCACCTCTGTAT
ABCC11	GGCTGAGCTACTGGTTGGAG	TGGTGAAAATCCCTGAGGAG
ABCC12	GGTGTTCATGCTGGTGTTTGG	GCTCGTCCATATCCTTGGAA
ABCG2	TATAGCTCAGATCATTGTCACAGTC	GTTGGTCGTCAGGAAGAAGAG
ERCC2	CTCAAGGAGCTGGCTAAGATGT	CATAGGCCTTGTAGGTCTCCAG
XRCC1	CATCGTGCGTAAGGAGTGGGTG	CCTGCTTCTCATAGAAGTTGAGC
Mcl-1	CGCCAAGGACACAAAGCC	GTCTCGTGGTTGCGCTGC
BRCA-1	GCCAGAAAACACCACATCAC	CAGTGTCCGTTCACACACAA
BRCA-2	CTCTGCCCTTATCATCGCTTTTC	TTTTGCTGCTTCCTTTTCTTCCT
E-cadherin	TACACTGCCCAGGAGCCAGA	TGGCACCAGTGTCCGGATTA
Vimentin	TGAGTACCGGAGACAGGTGCAG	TAGCAGCTTCAACGGCAAAGTTC
N-cadheirn	CGAATGGATGAAAGACCCATCC	GGAGCCACTGCCTTCATAGTCAA
Fibronectin	CCCAGACTTATGGTGGCAATTC	AATTCCGCCTCGAGTCTGA
MMP-2	GATAACCTGGATGCCGTCGTG	CTTCACGCTCTTGAGACTTTGGTTC
MMP-9	GCCCTGGAACTCACACGACA	TTGGAAACTCACACGCCAGAAG
α-SMA	CAGGATGCAGAAGGAGATCA	TCCACATCTGCTGGAAGGTA
Slug	TTCGGACCCACACATTACCT	GCAGTGAGGGCAAGAAAAAG
Snail	GACCACTATGCCGCGCTCTT	TCGCTGTAGTTAGGCTTCCGATT
Twist	GGAGTCCGCAGTCTTACGAG	TCTGGAGGACCTGGTAGAGG
ZEB1	TACAGAACCCAACTTGAACGTCACA	GATTACACCCAGACTGCGTCACA
ZEB2	TGACCTGCCACCTGGAACTCC	ACTTGATGTGCTCCTTCAGTGATGTC
β-Catenin	GCGTTCTCCTCAGATGGTGTC	CCAGTAAGCCCTCACGATGAT
STAT3	ACATTCTGGGCACAAACACA	CAGTCACAATCAGGGAAGCA
GAPDH	GCACCGTCAAGGCTGAGAAC	TGGTGAAGACGCCAGTGGA

with brown cytoplasm, nucleus, or membrane were considered positive. These cells were scored and then classified into the following four classes: none (0), weak brown (1+), moderate brown (2+), and strong brown (3+). The percentage of the stained tumor cells was divided into the following five classes: 0 for negative cells, 1 for 1%–25%, 2 for 25%–50%, 3 for 50%–75%, and 4 for >75%. The multiplication (staining index) of the intensity and percentage scores was used to determine the result.

Proteomic Analysis

Cells were sonicated three times on ice using a high-intensity ultrasonic processor (Ningbo Scientz Biotechnology Co. Ltd., Zhejiang, China) in lysis buffer (8 M urea, 1% protease inhibitor cocktail). After $12,000 \times g$ at 4°C for 10 min, protein concentration was determined with a BCA kit (Beyotime Institute of Biotechnology) according to the manufacturer's instructions. For digestion, the protein solution was reduced with 5 mM dithiothreitol at 56°C for 30 min and alkylated

with 11 mM iodoacetamide for 15 min at room temperature in darkness. Triethylammonium bicarbonate buffer (TEAB) was added to dilute samples. Finally, trypsin was added at a 1:50 trypsin/protein mass ratio for the first digestion overnight and a 1:100 ratio for a second 4-h digestion. Subsequently, peptides were then desalted by a Strata X C18 SPE column (Phenomenex, Torrance, CA, USA), vacuum dried, dissolved in 0.5 M TEAB, and labeled based on the tandem mass tag kit. Briefly, 1 U of TMT reagent was dissolved in acetonitrile and added to peptides for incubation for 2 h at room temperature, followed by pooling, desalting, and drying by vacuum centrifugation. Agilent 300Extend C18 column [5-μm particles, 4.6-mm internal diameter (ID), 250-mm length] was used to fractionate peptides. Briefly, peptides were first separated with a gradient of 8% to 32% acetonitrile over 60 min into 60 fractions. Then they were combined into 18 fractions and subjected to vacuum drying. The peptides were dissolved in 0.1% formic acid (solvent A) and separated using EASY-nLC 1000 ultraperformance

liquid chromatography (UPLC; Thermo Fisher Scientific Inc., Waltham, MA, USA). The gradient was an increase from 6% to 23% solvent B (0.1% formic acid in 98% acetonitrile) over 26 min, 23%–35% in 8 min, climbing to 80% in 3 min, and holding at 80% for the last 3 min at a constant flow rate of 400 nl/min. The peptides were subjected to a nano electrospray ionization source followed by tandem mass spectrometry in Q Exactive Plus (Thermo Fisher Scientific Inc.) coupled online to the UPLC. The MS scan was set as 350, 800 m/z, and 70,000 resolution; the tandem mass spectrometry (MS/MS) scan was set as 100 m/z and 17,500 resolution. The automatic gain control was set at 5E4, and the data-dependent acquisition procedure was applied to data acquisition.

Statistical Analysis

Results were expressed as mean ± SD of three independent experiments unless otherwise specified. Data were analyzed by two-tailed unpaired Student's t-test between any two groups. One-way analysis of variance (ANOVA) was used to assess the difference of means among groups. These analyses were performed using GraphPad Prism Software Version 5.0 (GraphPad Software Inc., La Jolla, CA, USA). A value of $p < 0.05$ was considered statistically significant.

RESULTS

ERCC1 Maintains the Resistance Phenotype of Oxaliplatin-Resistant CRC Cells

We first identified the resistance phenotype of HCT116/OXA cells. No difference existed between the proliferation rate of HCT116/OXA cells and that of the parent cells. According to Figure 1A, the IC_{50} values of oxaliplatin against HCT116/OXA and its parent cell line were 31.6 and 5.1 μM, respectively, thereby indicating the resistance of the former cell line against oxaliplatin. Moreover, HCT116/OXA also displayed cross-resistance to cisplatin, which exerted an IC_{50} value of 18.7 μM against this cell line, much higher than that against HCT116 cells (6.3 μM). To investigate the mechanism underlying oxaliplatin resistance, the expression of drug-resistant proteins, including ATP-binding cassette transporters, DNA damage response proteins, and antiapoptosis proteins, in HCT116/OXA and its parent cell line was determined by TMT-based quantitative proteomic analysis. The results illustrated that several proteins were upregulated in HCT116/OXA cells, such as ERCC1, P53, ABCG2, etc. (Fig. 1B). Consistent with this, the upregulation of ERCC1 and the increased expression of ERCC1 gene were observed in WB assay and RT-PCR, respectively (Fig. 1C–E).

To validate the dominant role of ERCC1 overexpression in inducing drug resistance, the HCT116/OXA cells were transfected with the si-ERCC1, which significantly inhibited ERCC1 protein and gene expression according to Figure 1F and G. Importantly, the transfection with si-ERCC1 led to an enhancement in sensitivity of HCT116/OXA cells to oxaliplatin (si-NC: IC_{50} = 30.8 μM; si-ERCC1-1: IC_{50} = 18.4 μM; si-ERCC1-2: IC_{50} = 16.7 μM) and cisplatin (siNC: IC_{50}= 16.8 μM; si-ERCC1-1: IC_{50} = 8.3 μM; si-ERCC1-2: IC_{50} = 7.5 μM) (Fig. 1H). In addition, knockdown of ERCC1 enhanced sensitivity of HCT116 cells to oxaliplatin and cisplatin. Thus, our data demonstrated that upregulated ERCC1 expression played an important role in maintaining resistance phenotype.
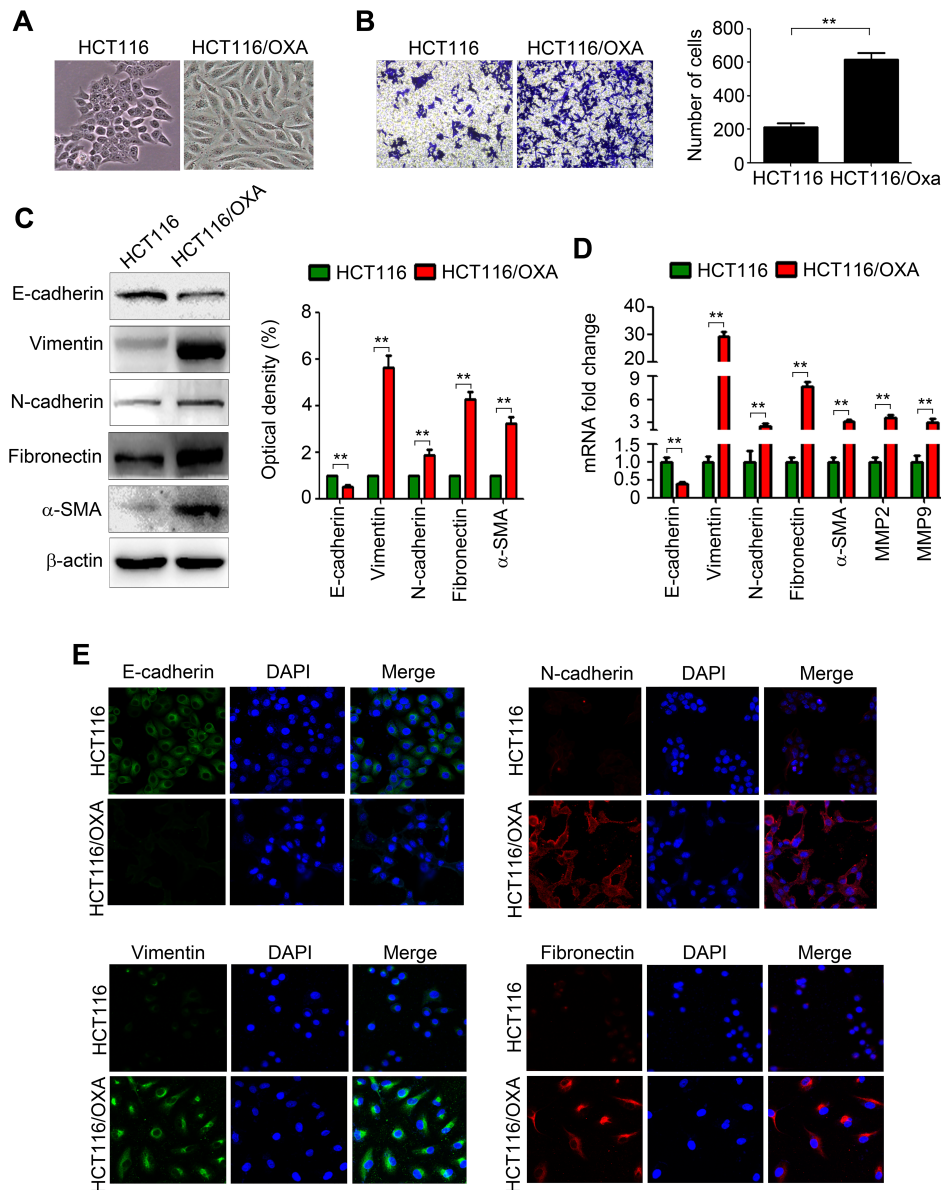
HCT116/OXA Cells Acquire the EMT Phenotype

In terms of the morphology, HCT116/OXA cells displayed fibroblastoid feature, while the susceptible cells exhibited an epithelial cobblestone appearance (Fig. 2A). These morphological differences indicated the development of EMT in resistant cells. As a result of the Transwell assay, HCT116/OXA cells exerted significantly enhanced migration capability compared with that of HCT116 cells (Fig. 2B). As illustrated by further WB assay, the epithelial maker E-cadherin was significantly downregulated, while the mesenchymal markers vimentin, N-cadherin, fibronectin, and α-smooth muscle actin (α-SMA) were upregulated in HCT116/OXA cells (Fig. 2C). RT-PCR demonstrated the decrease in E-cadherin gene expression, as well as the increase in vimentin, N-cadherin, fibronectin, α-SMA, matrix metallopeptidase 2 (MMP2), and MMP9 gene expression (Fig. 2D). Moreover, the decrease in E-cadherin expression, as well as the increase in vimentin, N-cadherin, and fibronectin expression, was confirmed by immunofluorescence staining (Fig. 2E). In conclusion, these results demonstrated that HCT116/OXA cells acquired EMT phenotype.

Slug Is Crucial for Aggressive Phenotype of HCT116/OXA Cells

The expression of an array of transcription factors was investigated to determine the one(s) mediating EMT of HCT116/OXA cells. According to WB assay, the upregulation of Slug, rather than Snail, Twist, ZEB1, STAT3, or β-catenin, occurred in HCT116/OXA cells (Fig. 3A). The upregulation of Slug mRNA expression was observed in RT-PCR (Fig. 3B). Considering transcription factors commonly function in the nucleus, we next separated the nucleus from the cell for examining Slug expression. As shown in Figure 3C, the Slug expression in the nucleus of HCT116/OXA cells was significantly increased. The results from the laser scanning confocal microscopy further confirmed that the nuclear translocation of Slug was increased in HCT116/OXA cells (Fig. 3D). The role of Slug in maintaining the aggressive phenotype of HCT116/OXA cells was investigated. Consequently, suppression of Slug
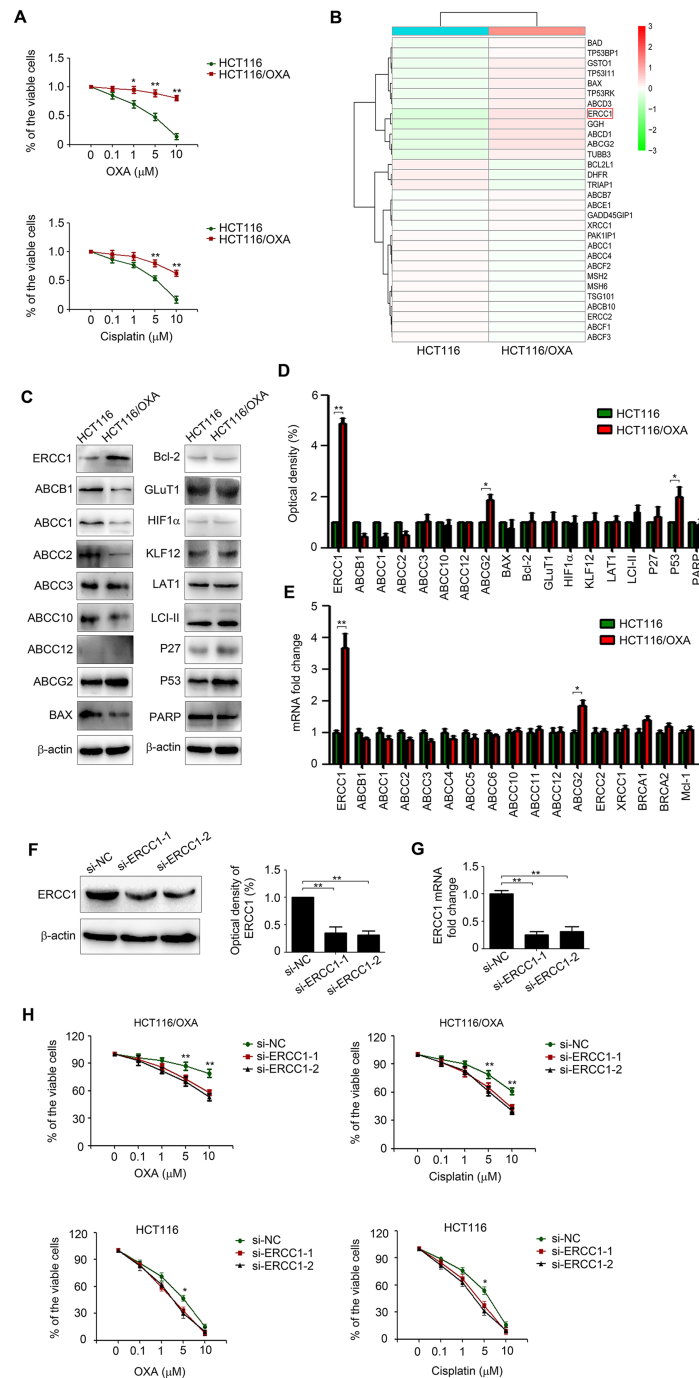
Figure 1. Excision repair cross-complementation group 1 (ERCC1) maintains the resistance phenotype of HCT116/OXA cells. (A) HCT116 and HCT116/OXA cells were treated with increasing concentrations of OXA or cisplatin for 48 h. Cell counting kit-8 (CCK-8) assay was used to quantify the viable cells. (B) Heat map of the expression levels of 30 drug resistance relative proteins. (C, D) The protein expression of ERCC1, ABCB1, ABCC1, ABCC2, ABCC3, ABCC10, ABCC12, ABCG2, BAX, Bcl-2, GluT-1, HIF1α, KLF12, LAT1, LCI-II, P27, P53, and PARP in HCT116 and HCT116/OXA cells was examined by Western blotting (WB). β-Actin served as the loading control. (E) The mRNA expression of ERCC1, ABCB1, ABCC1, ABCC2, ABCC3, ABCC4, ABCC5, ABCC6, ABCC10, ABCC11, ABCC12, ABCG2, ERCC2, XRCC1, BRCA1, BRCA2, and Mcl-1 in HCT116 and HCT116/OXA cells was examined by quantitative real-time polymerase chain reaction (RT-PCR). (F, G) Expressions of ERCC1 protein (F) and mRNA (G) in HCT116/OXA cells transfected with si-NC or si-ERCC1 for 24 h were detected by WB and quantitative RT-PCR, respectively. (H) HCT116/OXA and HCT116 cells transfected with si-NC or si-ERCC1 for 24 h were treated with increasing concentrations of OXA or cisplatin for 48 h. CCK-8 assay was used to quantify the viable cells. Data represented as means ± standard deviation (SD) were from three independent experiments. *$p < 0.05$, **$p < 0.01$. OXA, oxaliplatin; si-NC, negative control siRNA; si-ERCC1-1, ERCC1 siRNA 1; si-ERCC1-2, ERCC1 siRNA 2.

Figure 2. HCT116/OXA cells acquire epithelial–mesenchymal transition (EMT) phenotype. (A) Morphology of HCT116 and HCT116/OXA cells. (B) Transwell assay was performed to detect the migration of HCT116 and HCT116/OXA cells. (C) The protein expression of E-cadherin, vimentin, N-cadherin, fibronectin, and α-SMA in HCT116 and HCT116/OXA cells was examined by WB. (D) Quantitative RT-PCR was used to quantify E-cadherin, vimentin, N-cadherin, fibronectin, α-smooth muscle actin (α-SMA), matrix metallopeptidase 2 (MMP2), and MMP9 mRNA expression in HCT116 and HCT116/OXA cells. (E) The expression and cellular localization of E-cadherin, vimentin, N-cadherin, and fibronectin were analyzed by immunofluorescence staining. Nuclei were visualized with 4′,6-diamidino-2-phenylindole (DAPI) staining. Data represented as means ± SD were from three independent experiments. $**p < 0.01$.

increased E-cadherin expression and decreased vimentin, fibronectin, and ERCC1 expression at both mRNA and protein levels (Fig. 3E and F). Moreover, inhibition of Slug promoted the conversion from mesenchymal morphology to epithelial morphology (Fig. 3G), reduced migration ability (Fig. 3H), and enhanced sensitivity of HCT116/OXA cells to oxaliplatin (si-NC: $IC_{50} = 29.9$ µM; si-Slug-1: $IC_{50} = 13.1$ µM; si-Slug-2: $IC_{50} = 11.2$ µM) and cisplatin (si-NC: $IC_{50} = 16.1$ µM; si-Slug-1: $IC_{50} = 10.4$ µM; si-Slug-2: $IC_{50} = 8.2$ µM) (Fig. 3I). In addition, knockdown of Slug enhanced sensitivity of HCT116 cells to oxaliplatin and cisplatin. These results demonstrated that Slug was crucial for maintaining the aggressive phenotype.
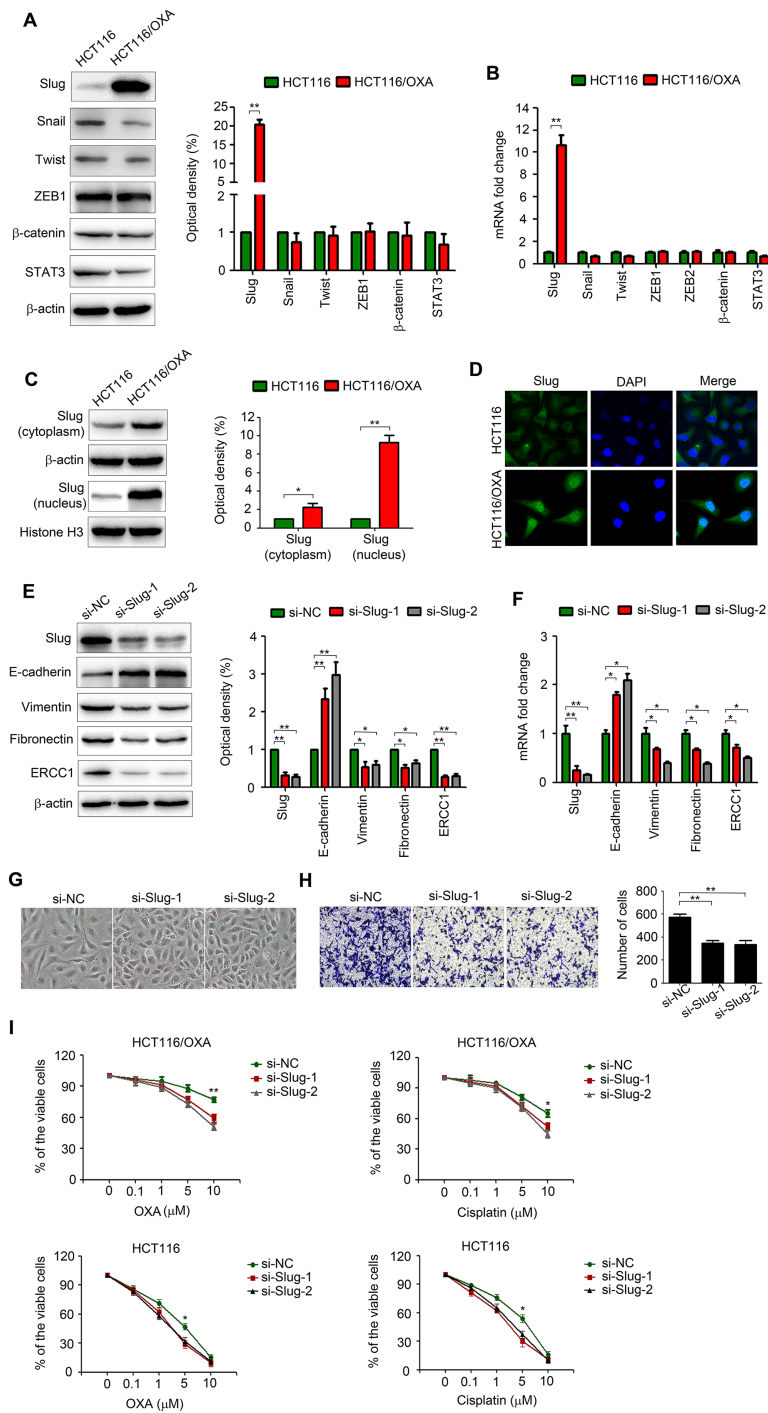
Figure 3. Slug is crucial for the aggressive phenotype of HCT116/OXA cells. (A, B) The protein (A) and mRNA (B) expression of Slug, Snail, Twist, ZEB1, β-catenin, and STAT3 in HCT116 and HCT116/OXA cells were examined by WB and quantitative RT-PCR, respectively. (C) The Slug expression in cytoplasm and nucleus in HCT116 and HCT116/OXA cells was examined by WB. (D) The cellar localization of Slug in HCT116 and HCT116/OXA cells was analyzed by immunofluorescence staining. Nuclei were visualized with DAPI staining. (E, F) Expression of Slug, E-cadherin, vimentin, fibronectin, and ERCC1 protein (E) and mRNA (F) in HCT116/OXA cells transfected with si-NC or si-Slug for 48 h were detected by WB and quantitative RT-PCR, respectively. (G) HCT116/OXA cells were transfected with si-NC or si-Slug for 48 h; cell morphological changes are shown in the phase contrast image. (H) HCT116/OXA cells were transfected with si-NC or si-Slug for 48 h; the migration capability was detected by Transwell assay. (I) HCT116/OXA and HCT116 cells transfected with si-NC or si-Slug for 24 h were treated with increasing concentrations of OXA or cisplatin for 48 h. CCK-8 assay was used to quantify the viable cells. Data represented as means ± SD were from three independent experiments. *$p <$ 0.05, **$p <$ 0.01. si-Slug-1, Slug siRNA 1; si-Slug-2, Slug siRNA 2.
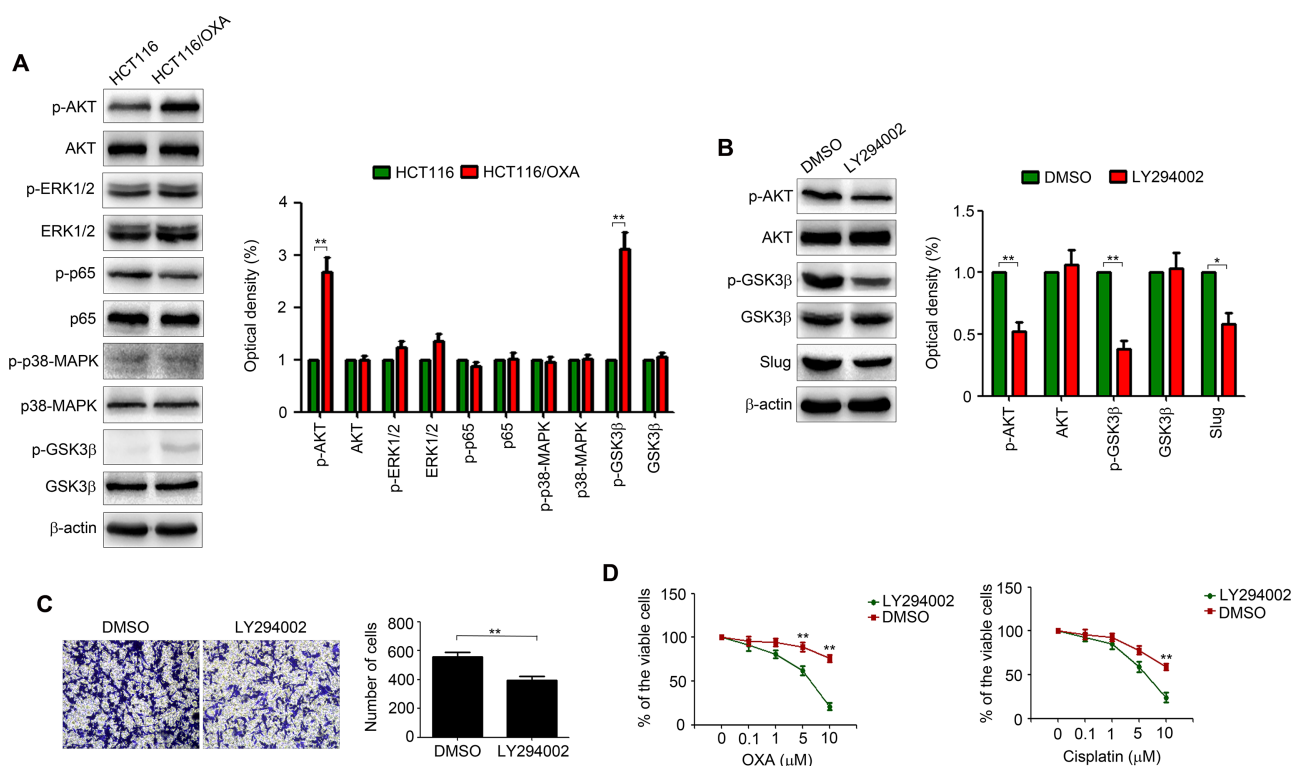
AKT Pathway Plays an Important Role in Regulating the Aggressive Phenotype of HCT116/OXA Cells

The AKT, extracellular signal-regulated kinase (ERK), p38-mitogen-activated protein kinase (MAPK), and nuclear factor (NF)-κB pathways were detected by WB for their critical role in regulating EMT and chemoresistance. The results showed that the AKT pathway was hyperactivated in HCT116/OXA (Fig. 4A). In addition, the phosphorylation of GSK3β, a kinase located downstream of the phosphatidylinositol 3-kinase (PI3K)/AKT pathway, was significantly upregulated (Fig. 4A). On the contrary, the exposure of HCT116/OXA cells to LY294002, a PI3K/AKT pathway inhibitor, culminated in the considerable downregulation of both pGSK3β and Slug (Fig. 4B). Additionally, LY294002 treatment decreased the migration capability of HCT116/OXA cells (Fig. 4C) and increased their sensitivity to oxaliplatin [dimethyl sulfoxide (DMSO): IC_{50} = 20.6 μM; LY294002: IC_{50} = 7.8 μM] and cisplatin (DMSO: IC_{50} = 13.7 μM; LY294002: $IC_{50}$ = 5.9 μM) (Fig. 4D). Taken together, these observations demonstrated that activated AKT signaling contributed to the aggressive phenotype of HCT116/OXA cells and increased Slug expression.

Oxaliplatin Promotes Expression and Nucleus Localization of Slug in CRC Cells

Following treatment with oxaliplatin for 0–6 h, Slug expression in HCT116 and SW480 cells was detected at both the mRNA and protein levels via RT-PCR and WB, respectively. As a result, oxaliplatin treatment upregulated Slug mRNA expression in a time-dependent manner, and this effect can be observed at 1 h postexposure (Fig. 5A). According to Figure 5B, the increase in protein level of Slug was observed at 4 h postexposure to oxaliplatin. Moreover, oxaliplatin treatment significantly increased Slug expression in the nucleus (Fig. 5C). This was further confirmed by the observation of increased Slug nuclear translocation in HCT116 cells with laser scanning confocal microscopy after oxaliplatin treatment (Fig. 5D).

Figure 4. AKT pathway is crucial for the aggressive phenotype of HCT116/OXA cells. (A) The protein expression of p-AKT, AKT, p-extracellular signal-regulated kinase 1/2 (ERK1/2), ERK1/2, p-p65, p65, p-p38-mitogen-activated protein kinase (MAPK), p38-MAPK, p-glycogen synthase kinase 3β (GSK3β), and GSK3β in HCT116 and HCT116/OXA cells was examined by WB. (B) HCT116 cells were treated with LY294002 (20 μM) for 24 h, and the expression of p-AKT, AKT, p-GSK3β, GSK3β, and Slug was examined by WB. (C) Transwell assay was performed to detect the migration of HCT116/OXA cells treated with LY294002 (20 μM) or dimethyl sulfoxide (DMSO) for 24 h. (D) HCT116/OXA cells were treated with LY294002 (20 μM) or DMSO for 24 h, and then treated with increasing concentrations of OXA or cisplatin for 48 h. CCK-8 assay was used to quantify the viable cells. Data represented as means ± SD were from three independent experiments. *$p < 0.05$, **$p < 0.01$.
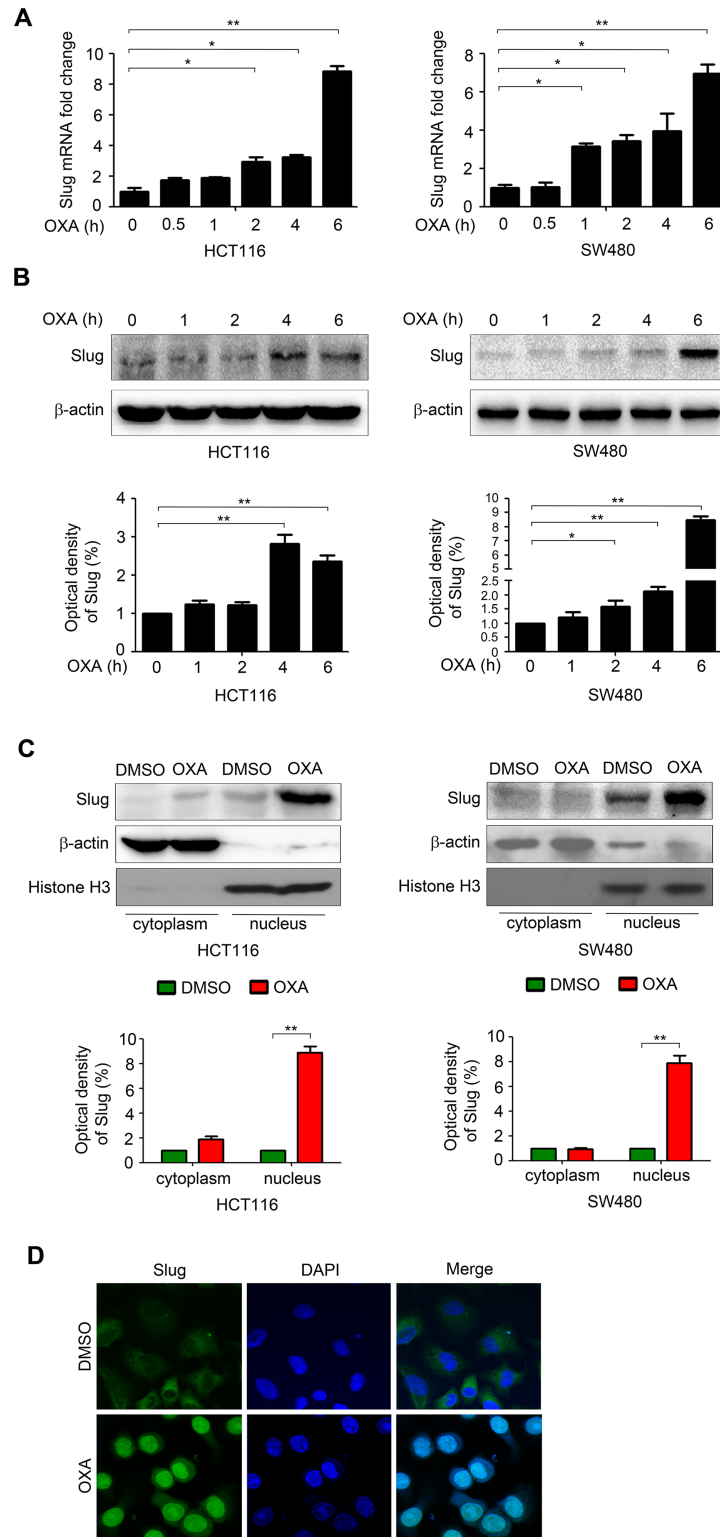
Figure 5. Oxaliplatin promotes expression and nucleus localization of Slug in colorectal cancer (CRC) cells. (A, B) HCT116 and SW480 cells were treated with OXA (25 μM) for the times indicated, and the protein (A) and mRNA (B) levels of Slug were examined by WB and quantitative RT-PCR, respectively. (C) HCT116 and SW480 cells were treated with OXA (25 μM) for 6 h, and the Slug expression in cytoplasm and nucleus was examined by WB. (D) The cellar localization of Slug in HCT116 treated with OXA (25 μM) for 6 h was analyzed by immunofluorescence staining. Nuclei were visualized with DAPI staining. Data represented as means ± SD were from three independent experiments. *$p < 0.05$, **$p < 0.01$.

Activation of AKT/GSK3β Signaling Is Involved in Oxaliplatin-Induced Slug Upregulation in CRC Cells

Oxaliplatin promoted the phosphorylation of AKT, ERK, p38-MAPK, and p65 in HCT116 and SW480 cells (Fig. 6A). To explore the specific pathway upregulating Slug expression, both cells lines were treated with BAY11-7082 (NF-κB inhibitor), LY294002, or SB-203580 (p38 inhibitor), and then with oxaliplatin. Following the drug treatment, Slug expression was determined by WB assay, which demonstrated LY294002 pretreatment resulted in the blockage of oxaliplatin-induced Slug upregulation (Fig. 6B). Hence, the PI3K/AKT pathway was responsible for this process. The activation of GSK3β via dephosphorylation was beneficial for Slug expression. Oxaliplatin promoted the phosphorylation of GSK3β in HCT116 and SW480 cells (Fig. 6A). On the contrary, LY294002 treatment reversed oxaliplatin-induced p-AKT, p-GSK3β, and Slug expression (Fig. 6C). Furthermore, suppression of GSK-3β by LiCl increased Slug expression (Fig. 6D). Taken together, these findings demonstrated that oxaliplatin treatment led to the activation of AKT signaling, which inhibited GSK3β and, consequently, upregulated Slug expression.

Slug and ERCC1 Are Upregulated in CRC Tissues and Predict Poor Survival of Patients

To validate the correlation of Slug and ERCC1 with the survival of CRC patients, we examined their expression in 74 cases of CRC tumor samples and 40 cases of normal tissues. As illustrated by immunohistochemistry, tumor samples exhibited an increase in both Slug and ERCC1 expression compared to the normal tissues (Fig. 7A–D). According to the bioinformatics analysis, the increased Slug mRNA expression was significantly correlated with the tumor size (Fig. 7E), lymph node metastasis (Fig. 7F), clinical stage grade (Fig. 7G), and Duke stage grade (Fig. 7H). CRC patients with increased expression of either Slug or ERCC1 displayed reduced overall survival (Fig. 7I–K). The results of Table 3 confirmed that Slug expression was significantly ($p < 0.05$) increased in higher-grade tumors. Importantly, we had observed the positive association of ERCC1 with Slug expression in CRC patients via immunohistochemistry (Fig. 8A and B) and the bioinformatics analysis (Fig. 8C). Collectively, both Slug and ERCC1 were upregulated in CRC tissues, which predicted poor survival of patients.

DISCUSSION

The existence of nonspecific and indistinct symptoms frequently delays the diagnosis of CRC, thereby rending the tumors nonresectable. Patients suffering from recurrent diseases after complete resection commonly need palliative treatment. However, a majority of patients achieve little or no benefit from adjuvant therapies, predominantly attributed to the development of chemoresistance[2,19]. Thus, there is a clear demand of effective strategies for addressing this issue. Elicited by the importance of oxaliplatin in CRC chemotherapy, we have recently undertaken the efforts to explore the mechanisms underlying the chemoresistance to this platinum anticancer agent.

Through mass spectrometry analysis and verification, we had identified the upregulation of ERCC1 in oxaliplatin-resistant HCT116 cells. As was known, DNA damage resulting from oxaliplatin treatment can be reversed by the nucleotide excision repair pathways. Since ERCC1 was a crucial protein participating in these pathways and it was correlated with the poor response of various cancers to the platinum anticancer agents[16,20], its role in mediating chemoresistance to oxaliplatin was studied in this research. After the knockdown of ERCC1, HCT116/OXA cells displayed enhanced sensitivity to both oxaliplatin and cisplatin. Although the knockdown of ABCG2, another multidrug-resistant protein slightly upregulated in HCT116/OXA cells, enhanced sensitivity of resistant cells to oxaliplatin and cisplatin (data not shown), the effect was less obvious than that caused by the knockdown of ERCC1. These experimental results demonstrated that the upregulation of ERCC1 expression was predominantly responsible for maintaining the resistance phenotype of HCT116/OXA cells, while the overexpression of ABCG2 merely played a subordinate role.

Chemoresistance is commonly accompanied with metastasis, thereby further neutralizing the therapeutic efficacy[21,22]. Mounting research has validated that drug-resistant cells tend to acquire EMT phenotype[23,24]. Consistent with this, HCT116/OXA cells were observed to acquire EMT phenotype and overexpressed Slug, a well-established transcription factor facilitating EMT[25–27]. On the contrary, silence of Slug gene reversed EMT phenotype of HCT116/OXA cells. Although other transcription factors, such as Snail, Twist, and ZEB1, were capable of inducing chemoresistance[5,28–30], no significant overexpression of them was identified in HCT116/OXA cells. To our knowledge, Slug contributed to the resistance against numerous antitumor drugs, as exemplified by EGFR inhibitors[31]. In particular, Slug also decreased sensitivity of CRC cells to 5-FU by suppressing miR145[32]. Similarly, our experimental results revealed that Slug was crucial for the development of drug resistance in HCT116/OXA cells. As a result of the knockdown of Slug, the ERCC1 expression was reduced in the resistant cells. This indicated the correlation of Slug expression and ERCC1 expression. According to a recent study, Snail contributed to cisplatin resistance in head and neck cancer by directly binding to ERCC1 promoter and increasing its expression[5]. Upon analyzing its sequence, we had observed four potential
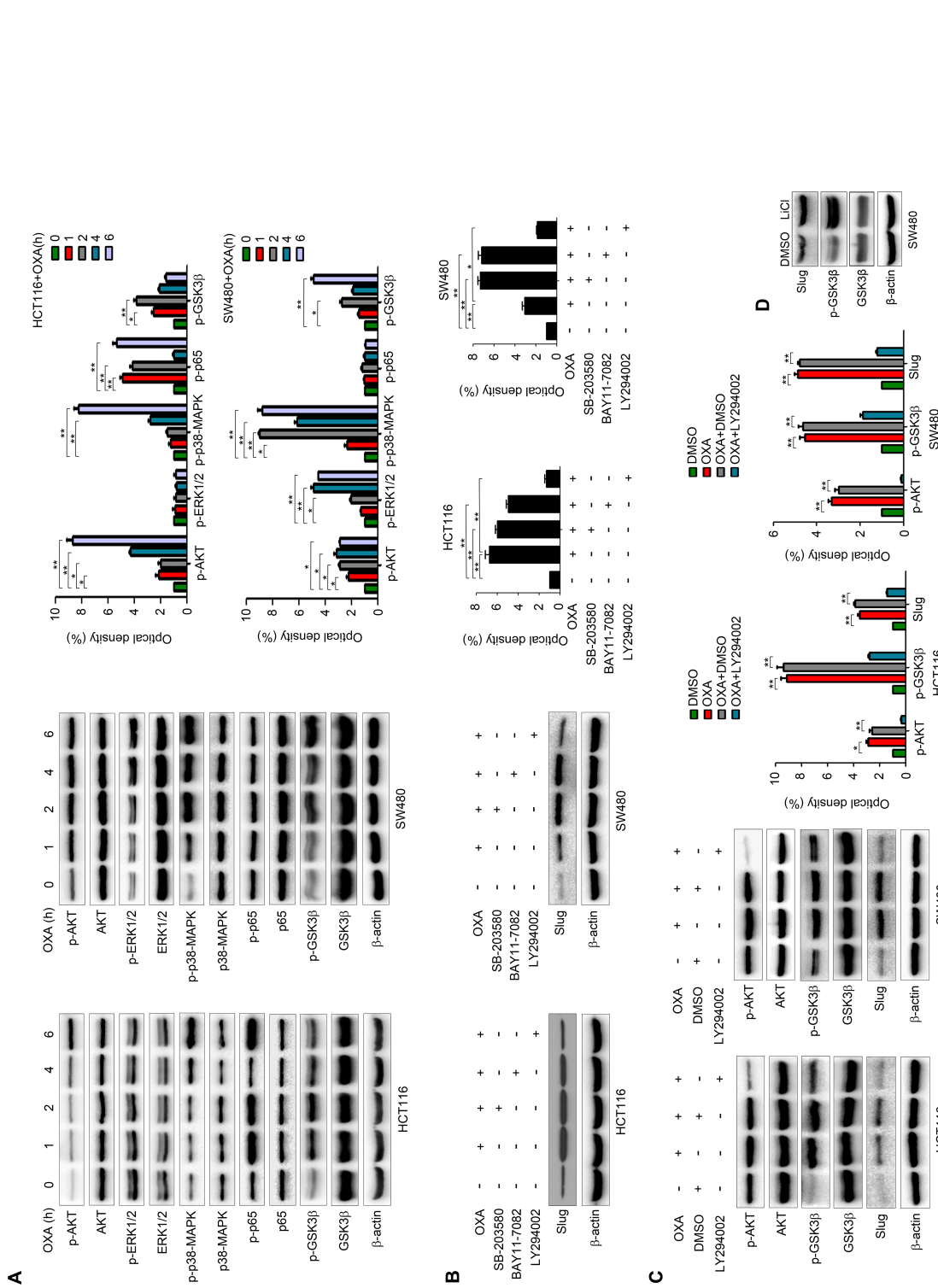
Figure 6. Oxaliplatin upregulates Slug through the AKT/GSK3β pathway. (A) HCT116 and SW480 cells were treated with OXA (25 μM) for the times indicated, and the protein expression of p-AKT, AKT, p-ERK1/2, ERK1/2, p-p65, p65, p-p38-MAPK, p38-MAPK, p-GSK3β, and GSK3β was examined by WB. (B) HCT116 and SW480 cells were pretreated with SB-203580 (20 μM), BAY11-7082 (10 μM), and LY294002 (20 μM) for 1 h, respectively, followed by stimulation with OXA (25 μM) for 6 h. The expression of Slug was examined by WB. (C) HCT116 and SW480 cells were pretreated with LY294002 (20 μM) or DMSO for 1 h, followed by stimulation with or without OXA (25 μM) for 6 h. The expression of Slug and the activation of AKT and GSK-3β were examined by WB. Data represented as means ± SD were from three independent experiments. (D) Expression of GSK-3β and Slug in SW480 cells treated with LiCl (40 mM) or DMSO for 24 h were detected by WB. *$p < 0.05$, **$p < 0.01$.
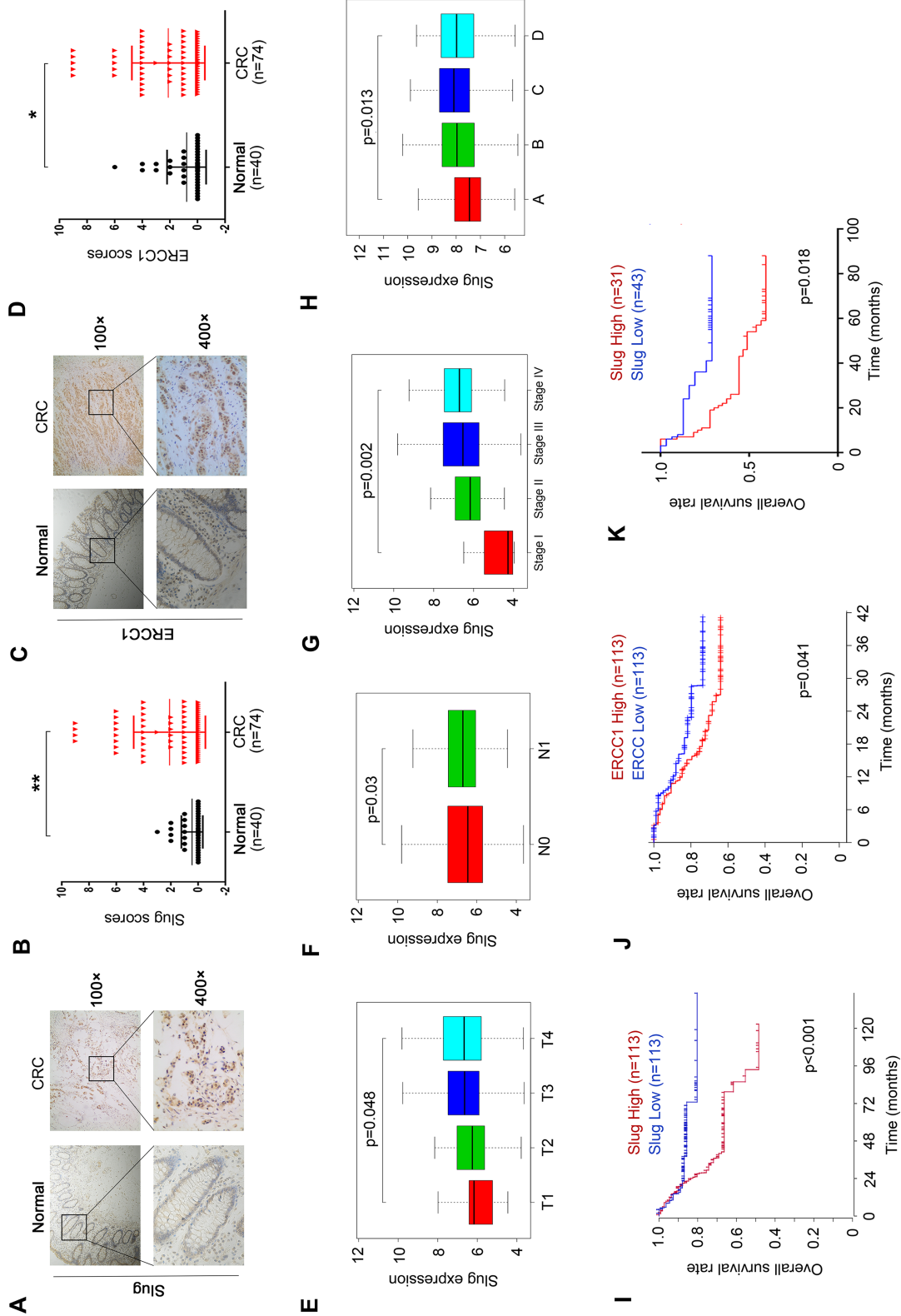
Figure 7. Slug and ERCC1 are upregulated in CRC tissues and predict poor survival of patients. (A, C) Representative immunohistochemical staining of Slug (A) and ERCC1 (C) in CRC tumor sample and normal tissue sample. (B, D) Scores for Slug (B) and ERCC1 (D) staining in 74 tumor tissue and 40 adjacent normal tissue samples from CRC patients. (E) Slug expression associates with tumor size in CRC patients in GSE39582 from the GEO database. (F) Association with Slug expression and lymph node metastasis in CRC patients in GSE39582 from the GEO database. N0: no lymph node metastasis; N1: lymph node metastasis. (G) The relative expression of Slug in stage I, II, III, and IV CRC patients based on data available in GSE39582 from the GEO database. (H) Slug expression associates with Duke stage grade in CRC patients in GSE14333 from the GEO database. (I, J) Impact of Slug and ERCC1 mRNA expression on overall survival in CRC patients in GSE14333 from the GEO database. (K) Univariate survival analysis of overall survival in 74 CRC patients as determined by Kaplan–Meier plot estimates based on Slug protein expression. *$p < 0.05$, **$p < 0.01$.

Table 3. Slug and ERCC1 Expression in Clinical and Pathological Characteristics of 74 Colorectal Cancer Patients

Variable Total	N	Expression of Slug in Cancer			Expression of ERCC1 in Cancer		
		Positive ($n = 43$)	Negative ($n = 31$)	p Value	Positive ($n = 44$)	Negative ($n = 30$)	p Value
Age				0.102			0.126
<50	16	12	4		12	4	
≥50	58	31	27		32	26	
Gender				0.378			0.199
Male	45	25	20		29	16	
Female	29	18	11		15	14	
Tumor size				0.512			0.376
<4	30	17	13		19	11	
>4	44	26	18		25	19	
Histological grade				**0.005**			0.320
I–II	61	31	30		35	26	
II–III	13	12	1		9	4	
Lymph node				0.057			0.476
Positive	33	23	10		19	14	
Negative	41	20	21		25	16	
Tumor stage				0.237			0.601
T1–T2	15	7	8		9	6	
T3–T4	59	36	23		35	24	

Slug binding sites on the ERCC1 promoter. Thus, it would be valuable to investigate whether Slug can directly bind to the ERCC1 promoter and promote its expression in a future study.

In our attempt to explore the signaling pathway mediating EMT and chemoresistance, we found the AKT pathway was upregulated in drug-resistant cells. Despite their capability to modulate EMT and drug resistance in different cancer cells[33–35], the upregulation of the ERK, NF-κB, and p38-MAPK pathways was not observed in this study. A recent study revealed that activation of IKKα by AKT induced Snail expression and promoted EMT[36].
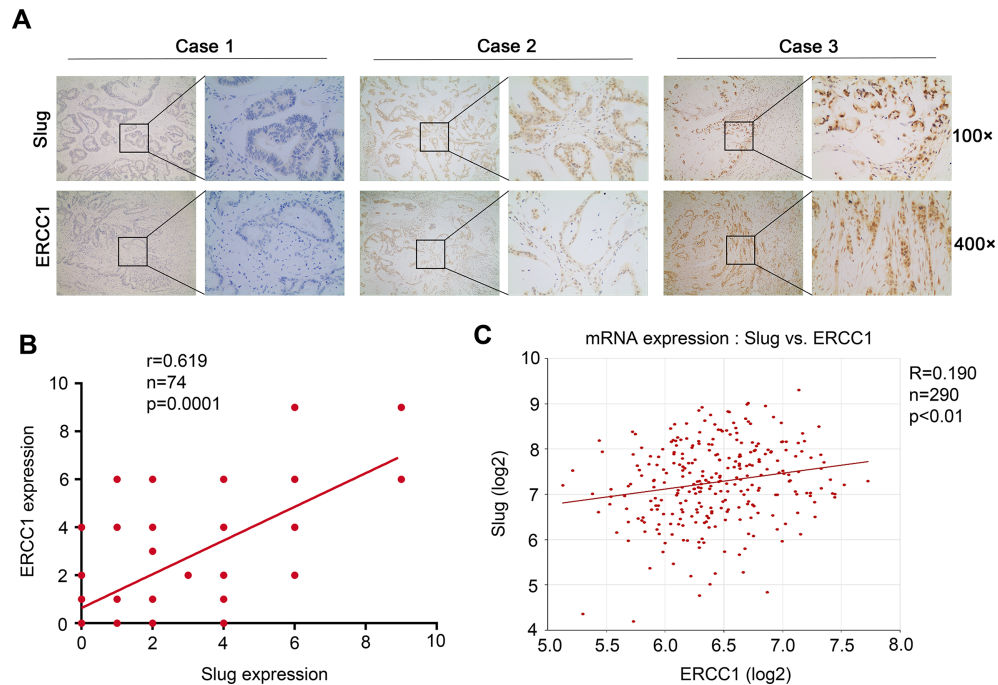
Figure 8. The expression of Slug and ERCC1 is significantly relative in CRC patients. (A) Representative immunohistochemical staining of Slug and ERCC1 in three CRC tissue samples. (B) Correlation between Slug and ERCC1 protein in 74 CRC patients. (C) The Pearson correlation between Slug and ERCC1 in 290 CRC tissue samples in GSE14333 from the GEO database.

Besides, AKT directly contributed to cisplatin resistance by regulating p53 action via the caspase-dependent mitochondrial death pathway[37]. Similarly, AKT signaling was proven to facilitate the development of chemoresistance in HCT116/OXA cells. The inhibition of AKT signaling by LY294002 dramatically inhibited the expression of Slug and enhanced the sensitivity of HCT116/OXA cells to oxaliplatin and cisplatin. The NF-κB, p38 MAPK, or ERK pathway may modulate EMT via affecting EMT transcription factor expression[38–40]. However, PI3K/AKT signaling rather than the aforementioned pathways was proven to mediate oxaliplatin-induced Slug upregulation. GSK3β, a downstream kinase of AKT, was characterized to be responsible for the subcellular location and expression of Slug[40,41]. Herein, we found that the activity of GSK3β was significantly reduced in HCT116/OXA cells and inhibition of GSK3β promoted Slug expression. Collectively, oxaliplatin treatment activated AKT signaling, repressed GSK3β activity, and inhibited the expression of Slug in CRC cells.

In summary, as revealed by this study, the activation of the AKT/GSK3β pathway upregulated Slug expression and further facilitated the development of resistance to oxaliplatin, as well as EMT. Hence, the simultaneous inhibition of the AKT/GSK3β/Slug axis may be of significance for surmounting metastasis and chemoresistance, thereby improving the therapeutic outcome of oxaliplatin.

REFERENCES

1. Jemal A, Bray F, Center MM, Ferlay J, Ward E, Forman D. Global cancer statistics. CA Cancer J Clin. 2011;61(2):69–90.
2. Liu T, Zhang X, Du L, Wang Y, Liu X, Tian H, Wang L, Li P, Zhao Y, Duan W, Xie Y, Sun Z, Wang C. Exosome-transmitted miR-128-3p increase chemosensitivity of oxaliplatin-resistant colorectal cancer. Mol Cancer 2019;18 (1):43.
3. Sun W, Li J, Zhou L, Han J, Liu R, Zhang H, Ning T, Gao Z, Chen X, Ba Y. The c-Myc/miR-27b-3p/ATG10 regulatory axis regulates chemoresistance in colorectal cancer. Theranostics 2020;10(5):1981–96.
4. Meng Q, Shi S, Liang C, Liang D, Hua J, Zhang B. Abrogation of glutathione peroxidase-1 drives EMT and chemoresistance in pancreatic cancer by activating ROS-mediated Akt/GSK3beta/Snail signaling. Oncogene 2018;37(44):5843–57.
5. Hsu DS, Lan HY, Huang CH, Tai SK, Chang SY, Tsai TL. Regulation of excision repair cross-complementation group 1 by Snail contributes to cisplatin resistance in head and neck cancer. Clin Cancer Res. 2010;16(18):4561–71.
6. Maseki S, Ijichi K, Tanaka H, Fujii M, Hasegawa Y, Ogawa T. Acquisition of EMT phenotype in the gefitinib-resistant cells of a head and neck squamous cell carcinoma cell line through Akt/GSK-3beta/snail signalling pathway. Br J Cancer 2012;106(6):1196–204.
7. Wang H, Zhang G, Zhang H, Zhang F, Zhou BH, Ning F. Acquisition of epithelial–mesenchymal transition phenotype and cancer stem cell-like properties in cisplatin-resistant lung cancer cells through AKT/beta-catenin/Snail signaling pathway. Eur J Pharmacol. 2014;723:156–66.
8. Arumugam T, Ramachandran V, Fournier KF, Wang H, Marquis L, Abbruzzese JL. Epithelial to mesenchymal transition contributes to drug resistance in pancreatic cancer. Cancer Res. 2009;69(14):5820–8.
9. Simeone P, Trerotola M, Franck J, Cardon T, Marchisio M, Fournier I. The multiverse nature of epithelial to mesenchymal transition. Semin Cancer Biol. 2018;58:1–10.
10. Phillips S, Kuperwasser C. SLUG: Critical regulator of epithelial cell identity in breast development and cancer. Cell Adh Migr. 2014;8(6):578–87.
11. Lin JC, Tsai JT, Chao TY, Ma HI, Liu WH. The STAT3/Slug axis enhances radiation-induced tumor invasion and cancer stem-like properties in radioresistant glioblastoma. Cancers (Basel) 2018;10(12).
12. Guo W, Keckesova Z, Donaher JL, Shibue T, Tischler V, Reinhardt F. Slug and Sox9 cooperatively determine the mammary stem cell state. Cell 2012;148(5):1015–28.
13. Kurrey NK, Jalgaonkar SP, Joglekar AV, Ghanate AD, Chaskar PD, Doiphode RY. Snail and slug mediate radioresistance and chemoresistance by antagonizing p53-mediated apoptosis and acquiring a stem-like phenotype in ovarian cancer cells. Stem Cells 2009;27(9):2059–68.
14. Ohmichi M, Hayakawa J, Tasaka K, Kurachi H, Murata Y. Mechanisms of platinum drug resistance. Trends Pharmacol Sci. 2005;26(3):113–6.
15. Siddik ZH. Cisplatin: Mode of cytotoxic action and molecular basis of resistance. Oncogene 2003;22(47):7265–79.
16. Urun Y, Leow JJ, Fay AP, Albiges L, Choueiri EK, Bellmunt J. ERCC1 as a prognostic factor for survival in patients with advanced urothelial cancer treated with platinum based chemotherapy: A systematic review and meta-analysis. Crit Rev Oncol Hematol. 2017;120:120–6.
17. Muallem MZ, Braicu I, Nassir M, Richter R, Sehouli J, Arsenic R. ERCC1 expression as a predictor of resistance to platinum-based chemotherapy in primary ovarian cancer. Anticancer Res 2014;34(1):393–9.
18. Lee HW, Choi YW, Han JH, Kim JH, Jung JH, Jeong SH. Expression of excision repair cross-complementation group 1 protein predicts poor outcome in advanced non-small cell lung cancer patients treated with platinum-based doublet chemotherapy. Lung Cancer 2009;65(3):377–82.
19. Jeong S, Kim BG, Kim DY, Kim BR, Kim JL, Park SH. Cannabidiol overcomes oxaliplatin resistance by enhancing NOS3- and SOD2-induced autophagy in human colorectal cancer cells. Cancers (Basel) 2019;11(6).
20. Bellmunt J, Paz-Ares L, Cuello M, Cecere FL, Albiol S, Guillem V. Gene expression of ERCC1 as a novel prognostic marker in advanced bladder cancer patients receiving cisplatin-based chemotherapy. Ann Oncol. 2007;18(3):522–8.
21. Chakraborty S, Kumar A, Faheem MM, Katoch A, Kumar A, Jamwal VL. Vimentin activation in early apoptotic cancer cells errands survival pathways during DNA damage inducer CPT treatment in colon carcinoma model. Cell Death Dis. 2019;10(6):467.
22. Siveen KS, Raza A, Ahmed EI, Khan AQ, Prabhu KS, Kuttikrishnan S. The role of extracellular vesicles as

modulators of the tumor microenvironment, metastasis and drug resistance in colorectal cancer. Cancers (Basel) 2019;11(6).

23. Choi HS, Kim YK, Yun PY. Up-regulation of MDR- and EMT-related molecules in cisplatin-resistant human oral squamous cell carcinoma cell lines. Int J Mol Sci. 2019;20 (12):3034.

24. Loret N, Denys H, Tummers P, Berx G. The role of epithelial-to-mesenchymal plasticity in ovarian cancer progression and therapy resistance. Cancers (Basel) 2019;11(6).

25. Ye X, Tam WL, Shibue T, Kaygusuz Y, Reinhardt F, Ng EE. Distinct EMT programs control normal mammary stem cells and tumour-initiating cells. Nature 2015;525 (7568):256–60.

26. Fang JH, Zhou HC, Zhang C, Shang LR, Zhang L, Xu J. A novel vascular pattern promotes metastasis of hepatocellular carcinoma in an epithelial–mesenchymal transition-independent manner. Hepatology 2015;62(2):452–65.

27. Liu X, Sun H, Qi J, Wang L, He S, Liu J. Sequential introduction of reprogramming factors reveals a time-sensitive requirement for individual factors and a sequential EMT-MET mechanism for optimal reprogramming. Nat Cell Biol. 2013;15(7):829–38.

28. Xiao G, Li Y, Wang M, Li X, Qin S, Sun X. FBXW7 suppresses epithelial–mesenchymal transition and chemoresistance of non-small-cell lung cancer cells by targeting snai1 for ubiquitin-dependent degradation. Cell Prolif. 2018;51(5):e12473.

29. Yochum ZA, Cades J, Wang H, Chatterjee S, Simons BW, O'Brien JP. Targeting the EMT transcription factor TWIST1 overcomes resistance to EGFR inhibitors in EGFR-mutant non-small-cell lung cancer. Oncogene 2019;38(5):656–70.

30. Sale MJ, Balmanno K, Saxena J, Ozono E, Wojdyla K, McIntyre RE. MEK1/2 inhibitor withdrawal reverses acquired resistance driven by BRAF(V600E) amplification whereas KRAS(G13D) amplification promotes EMT-chemoresistance. Nat Commun. 2019;10(1):2030.

31. Chang TH, Tsai MF, Su KY, Wu SG, Huang CP, Yu SL. Slug confers resistance to the epidermal growth factor receptor tyrosine kinase inhibitor. Am J Respir Crit Care Med. 2011;183(8):1071–9.

32. Findlay VJ, Wang C, Nogueira LM, Hurst K, Quirk D, Ethier SP. SNAI2 modulates colorectal cancer 5-fluorouracil sensitivity through miR145 repression. Mol Cancer Ther. 2014;13(11):2713–26.

33. Chiu LY, Hsin IL, Yang TY, Sung WW, Chi JY, Chang JT. The ERK–ZEB1 pathway mediates epithelial-mesenchymal transition in pemetrexed resistant lung cancer cells with suppression by vinca alkaloids. Oncogene 2017;36(2):242–53.

34. Shi G, Zheng X, Wu X, Wang S, Wang Y, Xing F. All-trans retinoic acid reverses epithelial–mesenchymal transition in paclitaxel-resistant cells by inhibiting nuclear factor kappa B and up-regulating gap junctions. Cancer Sci. 2019;110(1):379–88.

35. Milone MR, Pucci B, Bruzzese F, Carbone C, Piro G, Costantini S. Acquired resistance to zoledronic acid and the parallel acquisition of an aggressive phenotype are mediated by p38-MAP kinase activation in prostate cancer cells. Cell Death Dis. 2013;4(5):e641.

36. Julien S, Puig I, Caretti E, Bonaventure J, Nelles L, Van RF. Activation of NF-kappaB by Akt up-regulates Snail expression and induces epithelium mesenchyme transition. Oncogene 2007;26(53):7445–56.

37. Yang X, Fraser M, Moll UM, Basak A, Tsang BK. Akt-mediated cisplatin resistance in ovarian cancer: Modulation of p53 action on caspase-dependent mitochondrial death pathway. Cancer Res. 2006;66(6):3126–36.

38. Wu Y, Deng J, Rychahou PG, Qiu S, Evers BW, Zhou BP. Stabilization of snail by NF-kappaB is required for inflammation-induced cell migration and invasion. Cancer Cell 2009;15(5):416–28.

39. Storci G, Sansone P, Mari S, D'Uva G, Tavolari S, Guarnieri T. TNFalpha up-regulates SLUG via the NF-kappaB/HIF1alpha axis, which imparts breast cancer cells with a stem cell-like phenotype. J Cell Physiol. 2010;225 (3):682–91.

40. Tsai CC, Chou YT, Fu HW. Protease-activated receptor 2 induces migration and promotes Slug-mediated epithelial–mesenchymal transition in lung adenocarcinoma cells. Biochim Biophys Acta Mol Cell Res. 2019;1866 (3):486–503.

41. Kao SH, Wang WL, Chen CY, Chang YL, Wu YY, Wang YT. GSK3β controls epithelial–mesenchymal transition and tumor metastasis by CHIP-mediated degradation of Slug. Oncogene 2014;33(24):3172–82.